Environmental Science & Technology

pubs.acs.org/est

Article

Nitrification Regulates the Spatiotemporal Variability of N_2O Emissions in a Eutrophic Lake

Xia Liang,*,# Baoli Wang,# Dengzhou Gao, Ping Han, Yanling Zheng, Guoyu Yin, Hongpo Dong, Yali Tang, and Lijun Hou*

Cite This: https://doi.org/10.1021/acs.est.2c03992

Read Online

ACCESS | Metrics & More | Article Recommendations | Supporting Information

ABSTRACT: Nitrous oxide (N_2O) emissions from lakes exhibit significant spatiotemporal heterogeneity, and quantitative identification of the different N_2O production processes is greatly limited, causing the role of nitrification to be undervalued or ignored in models of a lake's N_2O emissions. Here, the contributions of nitrification and denitrification to N_2O production were quantitatively assessed in the eutrophic Lake Taihu using molecular biology and isotope mapping techniques. The N_2O fluxes ranged from −41.48 to 28.84 μmol m^{-2} d^{-1} in the lake, with lower N_2O concentrations being observed in spring and summer and significantly higher N_2O emissions being observed in autumn and winter. The ^{15}N site preference and relevant isotopic evidence demonstrated that denitrification contributed approximately 90% of the lake's gross N_2O production during summer and autumn, 27−83% of which was simultaneously eliminated via N_2O reduction. Surprisingly, nitrification seemed to act as a key process promoting N_2O production and contributing to the lake as a source of N_2O emissions. A combination of N_2O isotopocule-based approaches and molecular techniques can be used to determine the precise characteristics of microbial N_2O production and consumption in eutrophic lakes. The results of this study provide a basis for accurately assessing N_2O emissions from lakes at the regional and global scales.

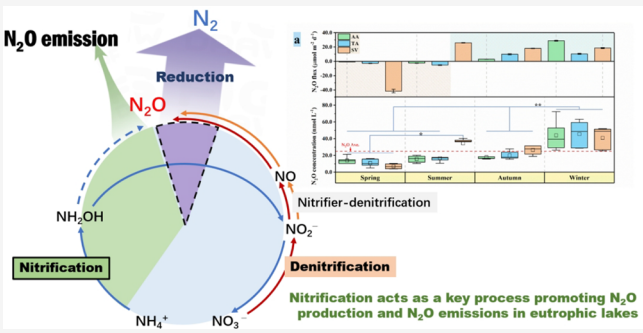

KEYWORDS: *nitrous oxide, nitrification, eutrophic lake, spatiotemporal variability*

1. INTRODUCTION

Nitrous oxide (N_2O) is an important greenhouse gas that has attracted much attention in recent climate change studies.[1] With increased anthropogenic reactive nitrogen inputs and nitrogen accumulation, quantifying N_2O budgets has become a popular and challenging topic in lake research.[2,3] However, the remarkable spatiotemporal heterogeneity of lake N_2O emissions makes it difficult to accurately determine lake N_2O budgets at the regional and global scales. Nitrification and denitrification are the main N_2O production pathways,[4,5] but the contributions of these two pathways of N_2O emissions vary significantly due to the spatial and temporal variability of the environmental factors and microbes, leading to inconsistencies in estimations of N_2O emissions at the field and regional scales.[6−8] Therefore, a method of precisely quantifying microbial N_2O sources is urgently needed to improve N_2O emission estimates, despite the existence of empirical methods for the estimation of N_2O emissions using environmental parameters (e.g., water temperature and nitrate content).[9,10]

Molecular biological techniques and isotopocule-based approaches have been widely applied in the recognition of key functional microorganisms and the simultaneous quantitative evaluation of the key microbial pathways (e.g., fungal- and bacterial-mediated denitrification) regulating N_2O production and consumption.[11−15] For example, denitrification has been reported to contribute to more than 90% of soil N_2O production in temperate coniferous forests and estuarine intertidal sediments, but most of this N_2O (up to 98%) is simultaneously eliminated in the soil layers via N_2O reduction, causing forest soils and tidal flats to exhibit low or negative N_2O fluxes and to serve as N_2O sinks.[4,16−18] In freshwater ecosystems, it has been found that the contribution of denitrification to N_2O emissions increases with increasing eutrophication level.[5,19] However, N_2O produced via nitrification has been found to contribute to the substantial N_2O accumulation in a coastal upwelling system and some lakes when suitable conditions occur, and it is thus a principal source of N_2O emissions in these water bodies.[20,21] In lakes, the contribution of nitrification to the gross N_2O emissions varies

Received: June 12, 2022
Revised: October 4, 2022
Accepted: October 20, 2022

ACS Publications © XXXX American Chemical Society

significantly (ranging from 20% to 100%) and depends on the trophic status and hypoxic conditions.[22,23] However, nitrification has been ignored or underestimated in models of the spatial and temporal variations in N_2O emissions from lakes. Currently, our understanding of the various microbial pathways regulating N_2O emissions from lakes is still limited, mostly due to a lack of quantitative information about the contributions of the different pathways to N_2O production and the potential N_2O reduction processes. This lack of quantitative information also makes it difficult to accurately characterize the underlying mechanisms controlling the N_2O source−sink processes and to precisely describe and predict the spatiotemporal variations in the N_2O emissions.

Herein, we hypothesized that the N_2O produced via nitrification is an important source of N_2O and promotes the spatiotemporal heterogeneity of N_2O emissions from eutrophic lakes. Lake Taihu in eastern China was selected as a representative lake to investigate the N_2O flux and the contributions of the various pathways to the N_2O production and consumption in the lake. The objectives of this study were to identify the critical role of nitrification in N_2O production and to reveal the mechanisms controlling the spatiotemporal heterogeneity of N_2O emissions from eutrophic lakes. This study is of great significance in improving our understanding of N_2O production, and it provides a basis for assessing N_2O budgets and mitigating N_2O emissions from lakes at regional and global scales.

2. MATERIALS AND METHODS

2.1. Site Description and Sample Collection. Lake Taihu is a typical shallow eutrophic lake in the middle and lower reaches of the Yangtze River Delta. The lake's surface area, mean depth, catchment area, and mean water retention time are 2338 km^2, 1.9 m, 36895 km^2, and 284 days, respectively.[24] The multiyear average annual rainfall and the temperature are about 430 mm and 15.5 °C, respectively, and the rainfall is concentrated in the summer (May−September). A detailed description of the site is provided in the Supporting Information. The annual lake N_2O emissions range from 0.13 to 0.49 Gg N yr, and the N_2O flux varies across the watershed.[25−27] Excessive nutrient loadings and frequent severe algal blooms have been suggested to be the environmental factors controlling the spatiotemporal variations in the N_2O emissions, and denitrification is thought to be the main pathway regulating the N_2O production in the lake.[25,27] Nitrification has been observed to occur under seasonal hypoxic and anoxic conditions and has been considered to play a role only in providing substrates for denitrification.[28]

Seasonal sampling was performed in the autumn (October) of 2018 and in the winter (January), spring (May), and summer (August) of 2019. Three typical sites were surveyed within the northern (Meiliang Bay, the algal-type zone, denoted as AA), southeastern (Eastern Taihu Bay, the macrophyte-type zone, denoted as SV), and central areas (Central Lake Taihu, the transition area between the algal-type and macrophyte-type zones, denoted as TA) (Figure 1). Water profiles were sampled at 0.5 m intervals from the surface to the sediment−water interface at all of the sites. The water temperature (WT), pH, dissolved oxygen (DO) content, and chlorophyll a content (Chl-a) were measured *in situ* using a calibrated automated multiparameter profiler (Model YSI 6600; YSI Inc., Yellow Springs, OH, USA). Water samples in triplicate were collected for nutrient and isotopic analyses. The

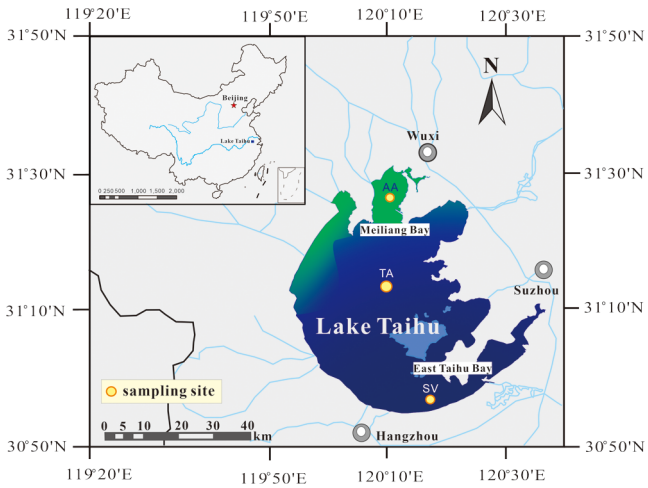

Figure 1. Sampling sites in the Taihu Lake. AA, TA, and SV denote the algal-type zone, the transition area between the algal-type and macrophyte-type zones, and the macrophyte-type zone, respectively. The solid yellow circles denote the sampling sites of the *in situ* surveys. The colors represent the algal distribution in Lake Taihu in May 2019, which were retrieved from remote sensing data (http://www.geodata.cn).

water samples used to measure the dissolved inorganic nitrogen (DIN, including ammonium, nitrate, and nitrite) and dissolved organic carbon (DOC) contents and isotopic composition were filtered using 0.45 μm cellulose acetate membranes (Millipore Corp., USA) within 12 h of collection. The filtered water samples were stored in 500 mL high-density polyethylene (HDPE) bottles at 4 °C for DIN and DOC analysis and in 200 mL black HDPE bottles at −20 °C for DIN isotopic analysis. The water samples for the isotopic analyses (i.e., $\delta^{18}O_{H_2O}$ and δD) were stored in 15 mL centrifuge tubes without headspace and were sealed with Parafilm-M. Water samples in quintuplicate were collected in 70 mL headspace bottles and 500 mL sampling bags for dissolved N_2O concentration and N_2O isotopic analyses, respectively, and they were preserved by adding saturated $HgCl_2$ and were sealed without headspace in the field. The water samples were stored in the dark at 4 °C for N_2O concentration analysis, and the samples for stable isotope analysis were frozen at −20 °C to prevent gas exchange with the atmosphere. The water sample for microbial DNA extraction was filtered using a 0.22 μm sterilized filter membrane (MF-Millipore, USA), and the membranes were then flash-frozen in liquid nitrogen and stored at −80 °C. The surface sediments (10 cm deep) were collected at each site using a rod hold sediment core sampler and were stored at −80 °C until they were analyzed. Further details regarding the sampling and treatment methods of the water and sediments to determine environmental parameters are presented in the Supporting Information.

2.2. Physical and Chemical Characteristics of Water and Sediment Samples. The total nitrogen (TN) and total phosphorus (TP) concentrations of the water samples were analyzed using ultraviolet spectroscopy after digestion in alkaline potassium persulfate and using molybdate spectrophotometry, respectively.[29] The ammonium (NH_4^+−N) concentration of the water samples were analyzed using Nessler's reagent, and the concentrations of nitrate (NO_3^-−N) and nitrite (NO_2^-−N) were quantified via ultraviolet−visible light (UV−vis) spectrophotometry. The measurements of the total

https://doi.org/10.1021/acs.est.2c03992
Environ. Sci. Technol. XXXX, XXX, XXX−XXX

organic carbon (TOC) and dissolved organic carbon (DOC) concentrations of the water samples were performed using an automatic elemental analyzer (Shimadzu TOC-V CPH, Shimadzu Co., Japan). To measure the sediment DOC, DIN, and orthophosphate (PO_4^{3-}), the sediment samples were centrifuged at 4000 rpm for 10 min to obtain the pore water, and then the pore water was filtered through a 0.45 μm filter for further analysis. The sediment samples used for TN, TP, and TOC analyses were dried at 70 °C for 48 h to determine the water content of the sediment. The dry sediments were then ground and sieved through a 100 mesh stainless steel sieve in preparation for nutrient analysis. The TN, TP, TOC, DOC, and DIN concentrations of the sediments were determined using the same method described above.

2.3. N_2O Concentration and Flux. The dissolved N_2O concentrations of the water samples were determined in triplicate using the headspace-equilibrium method described by Liang et al.[30] The N_2O concentration of the headspace was determined using a gas chromatograph (Shimadzu, GC-2014) equipped with an electron capture detector (ECD, HP6890) and a 4.5 m × 3 mm packed Porapak Q (80/100 mesh) column. The column and the ECD detector were conditioned at 50 and 320 °C, respectively. The N_2O concentration (C_{N_2O}, nmol L^{-1}) was calculated using the equation described by Goldenfum[31] and Mengis et al.[32]

$$C_{N_2O} = p_{N_2O} \times K \times 10^{-3} \quad (1)$$

where p_{N_2O} is the partial pressure of the N_2O in the water (μatm) and K is the solubility of N_2O at the laboratory temperature (mol L^{-1} atm^{-1}). The detailed calculation of p_{N_2O} is described in the Supporting Information. The flux of N_2O (F, μmol m^{-2} h^{-1}) was calculated using the equation described by Macintyre et al.[33]

$$F = k \times (C_{water} - C_{air}) \quad (2)$$

where C_{water} and C_{air} are the N_2O concentrations (C_{N_2O}) of the water and ambient air samples, respectively. k is the gas-exchange coefficient (cm h^{-1}), which was calculated by considering the wind speed and water temperature (the details are presented in the Supporting Information). The N_2O emissions (×10^3 kg N_2O−N yr^{-1}) from the lake were calculated by multiplying the average flux by the area of the lake.[34]

2.4. Isotopic Analysis. The nitrogen and oxygen isotopic compositions of the NH_4^+−N and NO_3^-−N ($\delta^{15}N_{NH_4^+}$, $\delta^{15}N_{NO_3^-}$ and $\delta^{18}O_{NO_3^-}$) were analyzed using the chemical conversion method with hypobromite and hydroxylamine oxidation and the bacterial denitrification method with *Pseudomonas aureofaciens*, respectively.[35,36] The $\delta^{18}O_{H_2O}$ value of the lake water was analyzed using a liquid water isotope analyzer (LGR, IWA-45EP, USA). The results are reported using the standard δ notation relative to Vienna Standard Mean Ocean Water (VSMOW). The analytical precision for $\delta^{18}O_{H_2O}$ is ±0.1‰. The isotopic analysis of the dissolved N_2O was conducted using a modified headspace-equilibrium method, and the isotopic composition of the N_2O was analyzed using a gas chromatograph-isotope ratio mass spectrometer (GC-IRMS, Thermo Fisher Scientific [China] Co., Ltd., Beijing, China).[11] The details of the modified headspace-equilibrium method and the IRMS calibration are presented in the Supporting Information.

The $\delta^{15}N^{bulk}$, $\delta^{18}O_{N_2O}$, $\delta^{15}N_{N2O}$, and site preference (SP) values were calculated using the methods of Toyoda and Yoshida[37] and Toyoda et al.[11]

$$\delta^{15}N^i = \frac{{}^{15}R^i_{sample}}{{}^{15}R_{std}} - 1 \quad (3)$$

$$\delta^{18}O = \frac{{}^{18}R_{sample}}{{}^{18}R_{std}} - 1 \quad (4)$$

$$\delta^{15}N^{bulk} = \frac{\delta^{15}N^\alpha + \delta^{15}N^\beta}{2} \quad (5)$$

$$SP = \delta^{15}N^\alpha - \delta^{15}N^\beta \quad (6)$$

where the isotopomer ratios of N ($\delta^{15}N^i$, i refers to α, β, or bulk) and O ($\delta^{18}O_{N_2O}$) are given in ‰, $\delta^{15}N^\alpha$ and $\delta^{15}N^\beta$ are the relative enrichments of ^{15}N in the central and terminal positions, respectively, and are reported relative to air,[38] ${}^{15}R^\alpha$ and ${}^{15}R^\beta$ represent the $^{15}N/^{14}N$ molar ratios at the center and end sites of the nitrogen atoms, respectively, ${}^{15}R^{bulk}$ and ${}^{18}R$ are the $^{15}N/^{14}N$ and $^{18}O/^{16}O$ isotope ratios, respectively, and R_{sample} and R_{std} are the isotope ratios of the sample and standard atmospheric N_2 for N and Vienna Standard Mean Ocean Water (V-SMOW) for oxygen, respectively. The difference between $\delta^{15}N^\alpha$ and $\delta^{15}N^\beta$ is referred to as the ^{15}N site preference (SP, in ‰).

2.5. Quantifying N_2O Production and Consumption. The $\delta^{15}N^{SP} - \delta^{18}O_{N_2O}$ mapping approach model (SP/O MAP) was used to estimate the contributions of the various pathways to the N_2O production and consumption. The corrected $\delta^{18}O_{N_2O}$ values, which were calculated based on the measured $\delta^{18}O_{H_2O}$ of the water from Lake Taihu and the corresponding isotope effect, were used as the nitrification (Ni) and denitrification (bD) mixing endmembers and the fractionation factors involved in the N_2O reduction.[15,39,40] One mixing line for the median values of Ni and bD and one reduction line with a mean slope were defined in the SP/O MAP. Two scenarios were used separately in the mapping models. (1) In the reduction-mixing scenario (R-M), the N_2O produced via bacterial denitrification is reduced, and the remaining N_2O is then mixed with the N_2O produced via nitrification. (2) In the mixing-reduction scenario (M-R), the N_2O produced via bacterial denitrification and nitrification is mixed, and the mixed N_2O is then reduced.[39,41] The impact of the fractionation associated with N_2O reduction and the admixture of N_2O originating from denitrification and nitrification were estimated according to the isotopic values of the samples and the calculated initial values on the isotopocule map.[40,42] A detailed summary and justification of the endmember values used, including relevant references, are presented in the Supporting Information.

The contributions of denitrification ($f_{bD\text{-gross}}$, %) and nitrification ($f_{Ni\text{-gross}}$, %) to the N_2O source and the degree of N_2O reduction (%) were calculated according to the method of Wu et al.[40] The fraction of the microbial-derived N_2O (f_{micro}, %) to the dissolved N_2O was calculated according to the method of Salk et al.[22] and Li et al.[5] The gross N_2O production rate ($N_2O_{production}$) and gross N_2O consumption

https://doi.org/10.1021/acs.est.2c03992
Environ. Sci. Technol. XXXX, XXX, XXX−XXX

Table 1. Physiochemical Parameters, N_2O Concentrations, N_2O Fluxes, and Isotopic Characteristics of the Water and Sediment Samples[a]

water			sediment		
param	value	*n*	param	value	*n*
WT (°C)	18.89 ± 1.07 (5.75, 31.92)	66	TP (g kg^{-1})	0.46 ± 0.03 (0.23, 0.78)	30
DO (mg L^{-1})	10.26 ± 0.25 (4.44, 13.59)	64	TN (g kg^{-1})	0.58 ± 0.05 (0.23, 1.19)	30
pH	8.46 ± 0.07 (8.00, 9.00)	47	TOC (mg L^{-1})	12.48 ± 0.48 (1.20, 27.93)	101
Chl-a (μg L^{-1})	12.61 ± 2.03 (2.79, 73.41)	64	DOC (mg L^{-1})	9.34 ± 0.39 (0.21, 20.81)	96
TP (mg L^{-1})	0.14 ± 0.01 (0.04, 0.28)	40	PO_3^+-P (mg L^{-1})	0.22 ± 0.04 (0.01, 2.76)	120
TN (mg L^{-1})	2.61 ± 0.25 (0.73, 5.88)	24	NH_4^+–N (mg L^{-1})	0.55 ± 0.05 (0.05, 3.37)	120
TOC (mg L^{-1})	9.76 ± 1.02 (2.32, 23.82)	40	NO_3^-–N (mg L^{-1})	0.72 ± 0.08 (0.05, 8.38)	122
DOC (mg L^{-1})	9.12 ± 0.92 (1.00, 24.42)	65	NO_2^-–N (mg L^{-1})	0.005 ± 0.01 (0.01, 0.12)	57
NH_4^+–N (mg L^{-1})	0.07 ± 0.01 (0.003, 0.42)	65			
NO_3^-–N (mg L^{-1})	0.61 ± 0.08 (0.06, 2.54)	65			
NO_2^-–N (mg L^{-1})	0.05 ± 0.01 (0.01, 0.66)	65			
C_{N_2O} (nmol L^{-1})	24.92 ± 1.94 (3.80, 72.24)	64			
N_2O flux (μmol m^{-2} d^{-1})	5.13 ± 5.39 (−41.48, 28.84)	12			
$\delta^{15}N_{NH_4^+}$(‰)	3.32 ± 0.27 (0.65, 9.96)	65			
$\delta^{15}N_{NO_3^-}$ (‰)	5.84 ± 0.42 (−4.76, 11.42)	65			
$\delta^{18}O_{NO_3^-}$ (‰)	7.91 ± 0.81 (−9.05, 18.09)	65			
$\delta^{18}O_{H2O}$ (‰)	−4.88 ± 0.10 (−5.90, −4.0)	37			
$\delta^{15}N^{bulk}_{N_2O}$ (‰)	−1.45 ± 0.23 (−4.49, 2.45)	64			
$\delta^{18}O_{N_2O}$ (‰)	27.06 ± 0.88 (14.39, 41.30)	64			
SP (‰)	9.81 ± 0.36 (4.83, 13.52)	31			

[a]The data are presented as the mean ± standard error, and the minimum and maximum values of the measurements are given in the parentheses; *n* indicates the sample numbers.

rate ($N_2O_{consumption}$) were also calculated, in which both the N_2O flux (μmol m^{-2} h^{-1}) and N_2O concentration (nmol L^{-1}) of the lake water were considered.[18] The details are presented in the Supporting Information.

2.6. Metagenomic Sequencing and Data Processing. The microbial DNA was extracted from the filters and sediments (0.5 g) using an E.Z.N.A. water and soil DNA Kit (Omega Biotek, Norcross, GA, US). The paired-end sequencing was performed using an Illumina NovaSeq/Hiseq Xten (Illumina Inc., San Diego, CA, USA) and NovaSeq Reagent Kits/HiSeq X Reagent Kits. The raw reads from the metagenomic sequencing were used to generate clean reads by removing adaptor sequences and trimming and removing low-quality reads using fastp (version 0.20.0).[43] A nonredundant gene catalog was constructed using CD-HIT (version 4.6.1),[44] with a 90% sequence identity and 90% coverage.

Representative sequences of the nonredundant gene catalog were annotated based on the US National Center for Biotechnology Information (NCBI-NR) database using blastp implemented in DIAMOND v0.9.19, with an e-value cutoff of $1e^{-5}$ and using Diamond (version 0.8.35) for the taxonomic annotations.[45] The cluster of orthologous groups of protein (COG) annotation for the representative sequences in each process of the nitrogen cycle (e.g., the *nif*H gene for nitrogen fixation) was performed using Diamond (version 0.8.35) against the evolutionary genealogy of genes: nonsupervised orthologous groups (eggNOG) database (version 4.5.1), with an e-value cutoff of $1e^{-5}$. Kyoto Encyclopedia of Genes and Genomes (KEGG) annotation was performed using Diamond (version 0.8.35) against the KEGG database (version 94.2), with an e-value cutoff of $1e^{-5}$.[45] The reads per kilobase million (RPKM) method was used to determine the relative abundances of each sample at the species, gene, and functional levels, and the functional composition and differences were analyzed. The dominant species, genes, and functional composition of the gene sets were intuitively studied using the histogram and heatmap visualization methods. The number of hits was normalized to the number per Gbps to compare the relative abundances of the nitrogen-cycle-related microbes in the different samples.

2.7. Statistics. The statistically significant differences among the sampling sites and seasons were analyzed using one-way analysis of variance (ANOVA) with least significant difference (LSD) and Tukey's honestly significant difference (HSD) test at significance levels of 0.05 and 0.001. Pearson's correlation analysis was used to analyze the correlations between the relative abundances of the microbial functional genes and the environmental parameters. The *t*-test was used to compare the linear regression slopes. The structural equation model (SEM) was used to account for the direct and indirect environmental variables that affected the N_2O concentration (see the Supporting Information for detailed calculations). The one-way ANOVA, Pearson's correlation analysis, and *t*-test were performed using the SPSS 18.0 statistical software package, and the statistical analyses involved in the SEM were performed using Amos Graphics software (version 22.0).

3. RESULTS

3.1. Water Physical and Chemical Parameters. The WT, DO, Chl-a, and DIN concentrations were 5.8–31.9 °C, 4.4–13.6 mg L^{-1}, 2.8–73.4 μg L^{-1}, and 0.15–2.65 mg L^{-1}, with mean values of 18.9 ± 1.01 °C, 10.26 ± 0.25 mg L^{-1}, 12.61 ± 2.03 μg L^{-1}, and 0.67 ± 0.20 mg L^{-1}, respectively (Table 1). High concentrations of Chl-a, DO, and DIN were observed in the spring and winter (Figures 2 and 3). The DO exhibited seasonal stratification in summer, and the lowest DO

https://doi.org/10.1021/acs.est.2c03992
Environ. Sci. Technol. XXXX, XXX, XXX−XXX

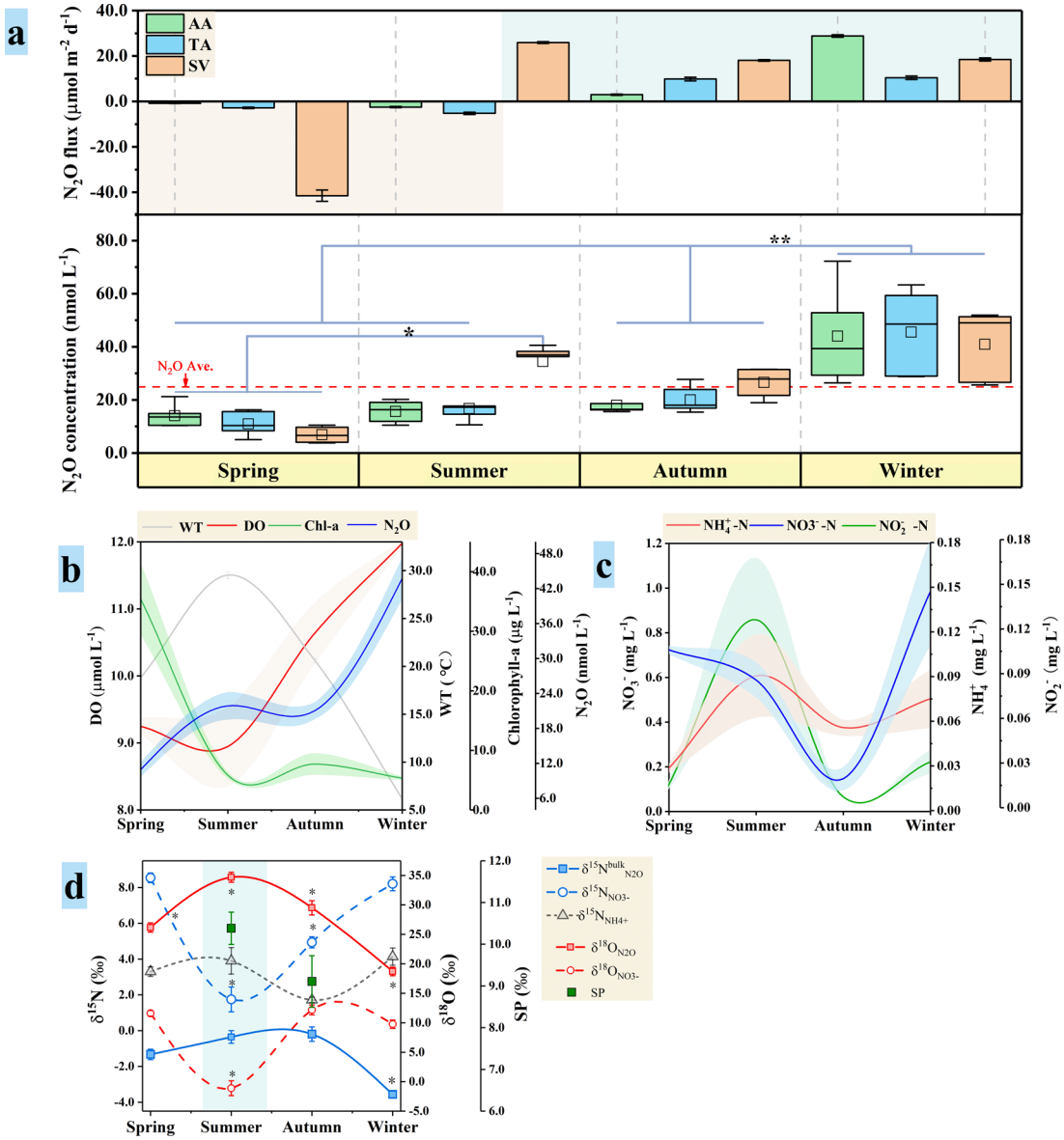

Figure 2. Temporal and spatial variations in the (a) N_2O fluxes and N_2O concentrations, (b) environmental parameters (water temperature, DO, and Chl-a), (c) water DIN (NH_4^+−N, NO_3^-−N, and NO_2^-−N) concentrations, and (d) isotopic compositions of N_2O, NO_3^-−N, and NH_4^+−N. For the N_2O concentration, the boxes and whiskers indicate the 25th to 75th and 10th and 90th percentiles, respectively, the asterisk denotes a statistically significant difference in the N_2O concentrations (* and ** denote significant differences at the $P < 0.05$ and $P < 0.001$ levels, respectively, using Tukey's HSD test), the red dashed line represents the average annual N_2O concentration of the water, and AA, TA, and SV denote the algal-type zone, the transition area between the algal-type and macrophyte-type zones, and the macrophyte-type zone, respectively. The data for the N_2O flux, environmental parameters, and DIN are presented as the mean ± standard error. For the isotopic compositions of N_2O, NO_3^-−N, and NH_4^+−N, the asterisk represents a statistical difference in the isotopic compositions between seasons ($P < 0.05$, LSD test).

concentration (4.44 mg L^{-1}) occurred at a water depth of 1.5 m in the AA area (Figure 3). The NO_3^-−N concentration of the water was observed to remain at a relatively high level throughout the year, while the NH_4^+−N concentration displayed a large range of values (from 0.001 to 0.42 mg L^{-1}), with the highest NH_4^+−N concentration being in the surface water in the SV area. High NH_4^+−N concentrations also occurred in the surface sediments in the AA area during winter, while NO_3^-−N accumulated in the surface sediments in the SV area in summer (Table S1).

3.2. Water N_2O Concentrations and N_2O fluxes. The dissolved N_2O concentrations ranged from 3.8 to 72.2 nmol L^{-1}, with an average of 27.9 ± 1.9 nmol L^{-1}, during the study period (Table 1). The N_2O concentrations increased from spring to winter, with remarkable N_2O stratification occurring in the winter (Figure 3). In addition, dramatic spatial variations in the N_2O concentrations occurred in the SV area where abnormally high N_2O concentrations were observed in summer. The N_2O fluxes ranged from −41.48 to 28.84 μmol m^{-2} d^{-1}, with an average N_2O flux and N_2O emissions of 5.13 ± 5.39 μmol m^{-2} d^{-1} and 0.19 Gg N yr^{-1}, respectively (Table 1). Low N_2O fluxes occurred in spring, while significantly high N_2O fluxes occurred in autumn and winter. In addition, the SV area exhibited large variations in the N_2O flux, which was the lowest (−41.48 μmol m^{-2} d^{-1}) in spring and the highest (25.93 μmol m^{-2} d^{-1}) in summer (Figure 2).

3.3. Isotopic Compositions and N_2O Source Partitioning. The $\delta^{15}N$ and $\delta^{18}O$ values of the NO_3^- ($\delta^{15}N_{NO_3^-}$ and

https://doi.org/10.1021/acs.est.2c03992
Environ. Sci. Technol. XXXX, XXX, XXX−XXX

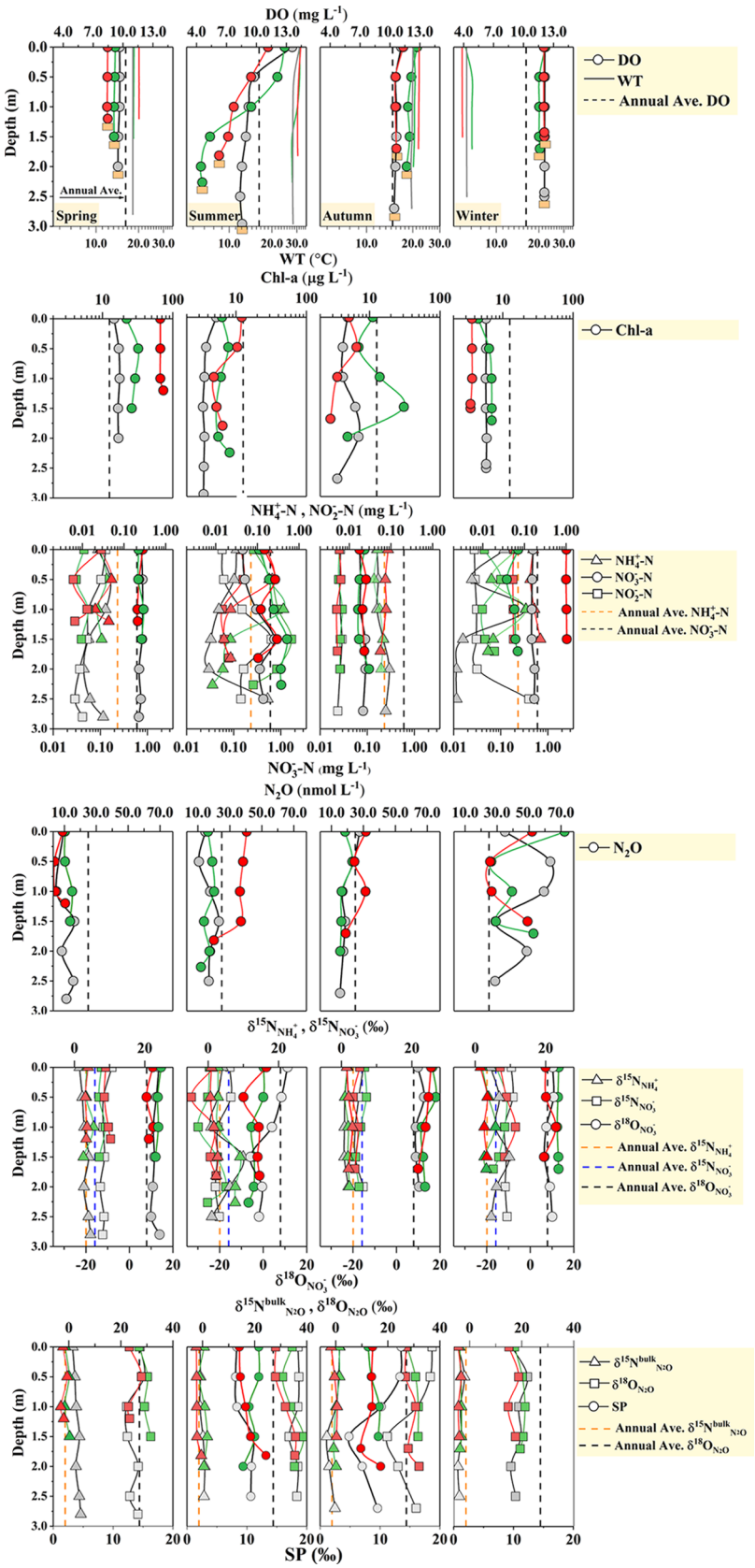

Figure 3. Variations in water temperature (WT), Chl-a, DO, DIN (NH_4^+–N, NO_3^-–N, NO_2^-–N), and N_2O concentrations, as well as the $\delta^{15}N^{bulk}$, $\delta^{15}N^{SP}$, and $\delta^{18}O$ values of the N_2O, and the $\delta^{15}N_{NO_3^-}$, $\delta^{18}O_{NO_3^-}$, and $\delta^{15}N_{NH_4^+}$ values of the water columns. The sediment–water interface is indicated by the solid yellow box. The dashed lines represent the average values of the parameters. AA, TA, and SV denote the algal-type zone, the transition area between the algal-type and macrophyte-type zones, and the macrophyte-type zone, respectively.

https://doi.org/10.1021/acs.est.2c03992
Environ. Sci. Technol. XXXX, XXX, XXX−XXX

Table 2. Isotopic Effects Associated with N_2O Production and Consumption[a]

item	factor	season	site	theor value	obsd value	adj r^2	p	n
N_2O Production								
Nitrification Occurs with Denitrification								
	$\delta^{18}O_{NO_3^-}$:$\delta^{15}N_{NO_3^-}$	sum	all sites	>1.0[b]	1.52 ± 0.30	0.63	<0.001	15
		aut	all sites		2.72 ± 0.42	0.79	<0.001	12
		win	TA + SV		1.17 ± 0.28	0.62	0.002	11
Denitrification								
	$\varepsilon^{15}N_{NO_3^-}$	sum	all sites	5−33[c]	4.08 ± 0.93	0.57	<0.001	15
N_2O Consumption								
	$\varepsilon^{15}N_{N_2O}$	sum	all sites	4−13[d]	3.86 ± 0.30	0.94	<0.001	11
		spr-aut-win	all sites		2.49 ± 0.63	0.51	0.002	15
	$\varepsilon^{18}O_{N_2O}$	sum	all sites	11−31[c]	9.49 ± 0.88	0.92	<0.001	11
		spr-aut-win	all sites		7.74 ± 1.95	0.51	0.002	15
	$\varepsilon^{18}O_{N_2O}$:$\varepsilon^{15}N_{N_2O}$	sum	all sites	2.5[d]	2.46			
		spr-aut-win	all sites		3.11			
	$\delta^{15}N^{SP}$:$\delta^{15}N_{N_2O}$	sum	AA	0.5−2.79[d](mean = 0.96)	1.56 ± 0.25	0.93	0.03	4
			SV		0.99 ± 0.09	0.98	0.01	4
		sum-aut	all sites		1.09 ± 0.27	0.45	<0.001	20

[a]$\varepsilon^{15}N_{NO_3^-}$ is the N isotope enrichment factor of NO_3^-−N, $\varepsilon^{15}N_{N_2O}$ and $\varepsilon^{18}O_{N_2O}$ are the N and O isotope enrichment factors of N_2O, and the ratio of $\delta^{15}N^{SP}$ to $\delta^{15}N_{N_2O}$ represents the N_2O reduction fractionation factor. Abbreviations: spr, spring; sum, summer; aut, autumn; win, winter. All sites mean the total sampling sites during the study periods. AA, TA, and SV denote the algal-type zone, the transition area between the algal-type and macrophyte-type zones, and the macrophyte-type zone, respectively. [b]From ref 50. [c]From ref 49. [d]From ref 38.

Table 3. Contributions of Microbial N_2O Production and Consumption[a]

					$N_2O_{production}$		$N_2O_{consumption}$	
modeling case	season	f_{micro} (%)	N_2O reduction (%)	$f_{bD\text{-}gross}$ (%)	nmol L^{-1}	μmol m^{-2} h^{-1}	nmol L^{-1}	μmol m^{-2} h^{-1}
R-M	summer	54.4 ± 1.8[a] (39.2, 68.2)	72.9 ± 1.7[a] (58.0, 83.6)	96.3 ± 0.5[Bb] (92.2, 99.3)	31.25 ± 4.20 (13.70, 69.49)	11.40 ± 16.53 (−6.77, 44.40)	9.40 ± 1.93 (2.34, 28.92)	5.34 ± 6.57 (−1.56, 18.48)
	autumn	64.6 ± 3.3[c] (41.8, 88.3)	60.8 ± 3.5[c] (27.6, 78.2)	94.3 ± 0.5[Ba] (90.5, 95.9)	37.02 ± 3.47 (23.34, 66.57)	16.80 ± 8.20 (5.19, 32.64)	15.56 ± 2.95 (7.13, 47.98)	6.52 ± 4.04 (2.23, 14.59)
M-R	summer	54.4 ± 1.8[a] (39.2, 68.2)	72.9 ± 1.7[a] (58.0, 83.6)	87.1 ± 1.3[A] (77.6, 96.7)	32.33 ± 4.38 (13.80, 72.15)	11.89 ± 17.13 (−6.84, 46.10)	10.48 ± 2.11 (2.75, 31.57)	5.83 ± 7.17 (−1.62, 20.17)
	autumn	64.6 ± 3.3[c] (41.8, 88.3)	60.8 ± 3.5[c] (27.6, 83.6)	85.0 ± 0.8[A] (79.9, 90.1)	38.31 ± 3.54 (24.22, 67.82)	17.52 ± 8.53 (5.36, 33.97)	16.84 ± 2.99 (8.60, 49.23)	7.23 ± 4.35 (2.41, 15.91)

[a]Results for two modeling cases: R-M is the reduction-mixing scenario; M-R is the mixing-reduction scenario. The data are presented as the mean ± standard error, and the minimum and maximum values of the measurements are provided in parentheses. The different capital letters on the mean values indicate significant differences among the different scenarios based on LSD ($P < 0.05$), and the different lower-case letters indicate significant differences among the seasons within each scenario.

$\delta^{18}O_{NO_3^-}$) and the $\delta^{15}N$ values of the NH_4^+ ($\delta^{15}N_{NH_4^+}$) ranged from 0.65 to 9.96‰, from −9.05 to 18.09‰, and from −4.76 to 11.42‰, respectively (Table 1). The $\delta^{15}N_{NO_3^-}$ and $\delta^{18}O_{NO_3^-}$ values exhibited significant seasonal variations, with lower values in summer and higher $\delta^{15}N_{NO_3^-}$ values in spring and winter (Figure 2d). Positive linear relationships were observed between $\delta^{18}O_{NO_3^-}$ and $\delta^{15}N_{NO_3^-}$ in all of the seasons, except for spring, and the $\delta^{15}N_{NO_3^-}$:$\delta^{18}O_{NO_3^-}$ ratio increased significantly in autumn (Table 2 and Figure S3). In addition, the $\delta^{15}N_{NO_3^-}$ value was found to increase with the natural log of the NO_3^-−N concentration in summer, and the slope of the linear regression (i.e., enrichment factor of $\delta^{15}N_{NO_3^-}$) was 4.08 ± 0.93‰ (Table 2 and Figure S3; details are presented in the Supporting Information).

For the water N_2O, the $\delta^{15}N^{bulk}$ and $\delta^{18}O_{N_2O}$ values ranged from −4.49 to 2.45‰ and from 14.39 to 41.30‰, with averages of −1.45 ± 0.23‰ and 27.06 ± 0.88‰, respectively. The lowest $\delta^{15}N^{bulk}$ and $\delta^{18}O_{N_2O}$ values occurred in winter, and the highest $\delta^{18}O_{N_2O}$ value occurred in summer (Figure 2). Linear relationships were observed between the isotopic compositions ($\delta^{15}N^{bulk}$ and $\delta^{18}O_{N_2O}$) and the inverse of the measured N_2O concentration in all of the seasons, and the highest value of the isotope effect (i.e., slope of the linear regression lines) occurred in summer ($\varepsilon^{15}N_{N_2O} \approx 3.9$‰ and $\varepsilon^{18}O_{N_2O} \approx 9.5$‰) (Table 2 and Figure S4). In addition, the $\varepsilon^{18}O_{N_2O}$:$\varepsilon^{15}N_{N_2O}$ ratio was close to 2.5 in summer, but the ratios in other seasons exhibited an obvious positive deviation (Table 2 and Figure S4). High spatiotemporal heterogeneity of the $\delta^{15}N^{SP}$ value was also observed in summer and autumn, during which high SP values (13.17‰) occurring in the SV area (Figure 3). In addition, using the isotope mapping approach, which employs dual isotope plots (i.e., $\delta^{15}N^{SP}$ and $\delta^{18}O_{N_2O}$) to constrain the N_2O reduction progress and endmember mixing ratios, it was found that approximately 77.6−99.3% of the gross N_2O production in the lake was

https://doi.org/10.1021/acs.est.2c03992
Environ. Sci. Technol. XXXX, XXX, XXX−XXX

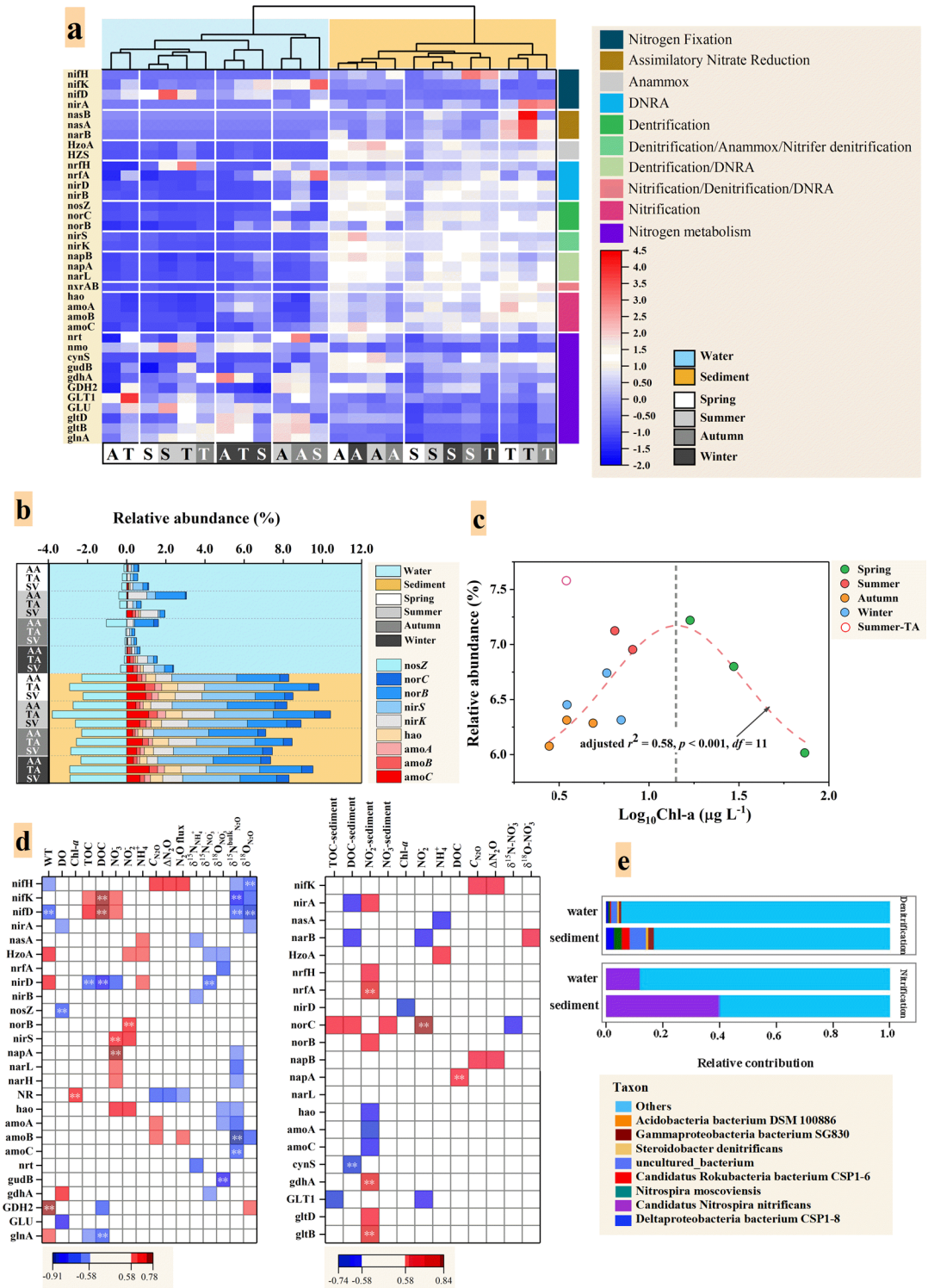

Figure 4. Functional annotation and relative abundances of the genes in the water and sediments. (a) Genes involved in nitrogen metabolisms. The heat map shows the relative abundances of the KEGG Orthology genes annotated using the KEGG database; A, T, and S denote the algal-type zone, the transition area between the algal-type and macrophyte-type zones, and the macrophyte-type zone, respectively. (b) Relative abundances of functional genes involved in N_2O production and consumption in the water (blue background) and sediments (yellow background). AA, TA, and SV denote the algal-type zone, the transition area between the algal-type and macrophyte-type zones, and the macrophyte-type zone, respectively. (c) Relationships between the relative abundances of denitrification genes (*nor*BC and *nirSK*) and Chl-a concentration at the sediment−water interface. (d) Spearman rank correlations between abundance (percent normalized gene abundance) of nitrogen-metabolism-related genes and measured environmental parameters in the water (left) and surface sediment (right; parameters unlabeled with sediment are for the sediment−water interface). All of the colored squares and the colored squares with a double asterisk (**) in the figure indicate $P < 0.05$ and $P < 0.001$ levels, respectively; the different colors indicate the type of correlation (Spearman's ρ; red being positive and blue being negative). (e) Relative contributions of the different taxa at the species levels to the nitrification and denitrification in the water and sediments.

https://doi.org/10.1021/acs.est.2c03992
Environ. Sci. Technol. XXXX, XXX, XXX−XXX

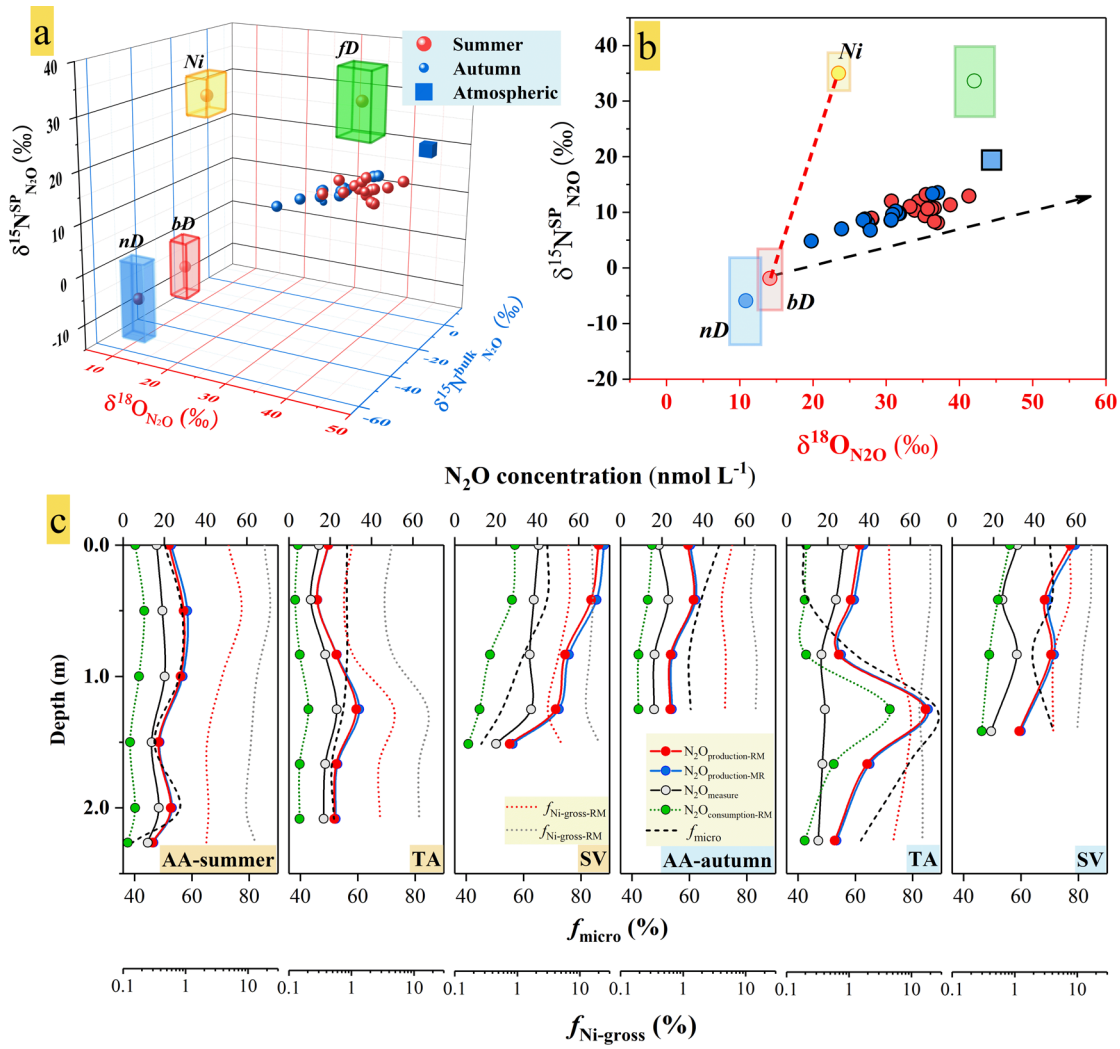

Figure 5. (a) 3-D map of $\delta^{15}N^{SP}$ (y axis), $\delta^{18}O$ (x axis), and $\delta^{15}N^{bulk}$ (z axis), (b) SP/O map, and (c) the modeled pathway fractions and the gross N_2O production and consumption. In (a), *bD* is bacterial denitrification, *nD* is nitrifier denitrification, *fD* is fungal denitrification, and *Ni* is nitrification. The solid blue square indicates atmospheric N_2O. The black and red dashed lines in (b) are the theoretical reduction line and the mixing line between denitrification and nitrification, respectively. In (c), RM is the reduction-mixing scenario, MR is the mixing-reduction scenario, and $N_2O_{measure}$ is the measured N_2O concentrations in the water columns. A detailed summary and justification of the endmember values are presented in the Supporting Information. AA, TA, and SV denote the algal-type zone, the transition area between the algal-type and macrophyte-type zones, and the macrophyte-type zone, respectively.

sourced from denitrification ($f_{bD\text{-}gross}$), 27−83% of which was simultaneously reduced to N_2 (Table 3 and Figure 5).

3.4. Metagenomic Analysis of Pathways Controlling the N_2O Flux. About 1106751748 paired-end clean reads were generated for a total of 24 water and sediment samples and were related to main nitrogen metabolic pathways, including nitrification, denitrification, nitrogen fixation, assimilated nitrate reduction, and dissimilated nitrate (Figure 4). The relative abundances of the microbial functional genes involved in N_2O production (*amo*, *hao*, and *nor*) and reduction (*nosZ*) were significantly higher in the surface sediments than in the water. Significant seasonal variations in the relative gene abundances were observed in the lake waters, with the highest abundance of nitrifying genes (*amoABC* and *hao*) occurring in winter and the maximum abundance of denitrifying genes (*nirSK*, *norBC*, and *nosZ*) occurring in summer (Figure 4b and Figure S2a). The relative abundances of functional genes in the surface sediments exhibited significant spatial variability, with the lowest nitrifying gene abundances occurring in the AA area and lower denitrifying gene abundances occurring in the SA area in spring. In addition, species and functional contribution analysis revealed that *Gammaproteobacteria*, *Steroidobacter denitrificans*, and *Candidatus Nitrospira nitrificans* (*Ca. N. nitrificans*) were the main contributors of denitrification and nitrification (Figure 4e and Figure S2). Furthermore, there was a significant positive correlation between the relative abundance of *amo*AB and the N_2O concentration ($r > 0.6$, $P < 0.05$), and there was a negative correlations between the relative abundance of *amo*BC and the $\delta^{15}N^{bulk}$ value in the water ($r^2 > 0.56$, $P < 0.005$; Figure 4d). In contrast, the relative abundances of the denitrifying functional genes (i.e., *nirSK* and *nor*BC) exhibited a unimodal relationship with the Chl-a concentration of the surface sediments (Figure 4c).

4. DISCUSSION

4.1. Key Processes related to N_2O Emissions. Excessive anthropogenic nitrogen input has made eutrophic lakes a hot spot for nitrogen removal and N_2O emissions.[27,46] In this

https://doi.org/10.1021/acs.est.2c03992
Environ. Sci. Technol. XXXX, XXX, XXX−XXX

study, the N_2O emissions exhibited significant seasonal variations, with low N_2O fluxes (-15.07 ± 13.22 μmol m^{-2} d^{-1}) in spring and significantly high values in winter (19.24 ± 5.34 μmol m^{-2} d^{-1}). The variations in the N_2O flux from negative values to positive values indicate a shift of the lake from an N_2O sink to a source.[32,47] These results are consistent with the results of previous studies that identified the temporal and spatial heterogeneity of N_2O emissions in Lake Taihu.[25−27]

Biotic nitrification and denitrification are considered to as the main N_2O production pathways, but denitrification is considered to play a more critical role than nitrification in regulating N_2O emissions because it is the only process that both produces and consumes N_2O.[4,5,48] To understand the mechanisms involved in the spatial−temporal variations in the N_2O flux, the main pathways of N_2O production and the N_2O consumption processes were qualitatively evaluated by investigating the relationship between $\delta^{15}N_{NO_3^-}$ and $\delta^{18}O_{NO_3^-}$ and the isotope enrichment factors associated with denitrification ($\varepsilon^{15}N_{NO_3^-}$) and N_2O consumption ($\varepsilon^{15}N_{N_2O}$ and $\varepsilon^{18}O_{N_2O}$) (the details are presented in the Supporting Information). Denitrification has been reported to have isotopic enrichment factors (i.e., $\varepsilon^{15}N_{NO_3^-}$) ranging from 5‰ to 33‰.[49] Nitrification is thought to co-occur with denitrification when the potential isotopic effect value (i.e., the ratio of $\delta^{15}N_{NO_3^-}$ to $\delta^{18}O_{NO_3^-}$) is >1.0.[50] In this study, the isotopic effects of the co-occurrence of nitrification and denitrification were observed in all of the seasons, except for spring, and significant isotope fractionation due to denitrification was only observed in the summer (Table 2 and Figure S3). Thus, it is reasonable to infer that nitrification co-occurred with denitrification in Lake Taihu, but the denitrification was more intense in the summer. Denitrification with strong N_2O reduction is thought to occur with an ^{18}O to ^{15}N enrichment ratio (i.e., $\varepsilon^{18}O_{N_2O}$:$\varepsilon^{15}N_{N_2O}$) of ∼2.5.[51] The positive deviation indicates a N_2O source with relatively low $\delta^{15}N^{bulk}$ values, which partially counteracts the isotopic signature of the N_2O consumption.[38,47] N_2O produced via nitrification generally has lower $\delta^{15}N^{bulk}$ values than that produced via denitrification.[52] As a result, the different enrichment ratio values in summer (close to 2.5) compared to the other seasons (obvious positive deviation to 2.5) suggest that N_2O consumption was the dominant force driving the low lake N_2O concentration in summer, and the co-occurrence of nitrification and denitrification may support more net N_2O accumulation by increasing the N_2O production and leading to higher lake N_2O concentration in autumn and winter. The mechanisms of N_2O production during nitrification were explored using an environmental factor analysis (i.e., SEM; the details are presented in the Supporting Information), which revealed that NH_4^+−N served as an important substrate for nitrification and increased the N_2O yield (Table S4 and Figure S6).

4.2. Microbial-Driven N_2O Production and Consumption Mechanisms. Algal blooms and the decay of excess algal biomass have been reported to inhibit denitrification in the sediments and thus N_2O emissions in Lake Taihu.[27,28] In this study, the lowest N_2O emissions from Lake Taihu occurred during the algal bloom in spring, which is consistent with previous studies on the lake. The lower lake N_2O concentrations and higher water Chl-a were accompanied by a decline in the relative abundances of the denitrifying functional genes in the water (i.e., *nir*SK and *nor*BC) and the *nos*Z gene in the surface sediments (Figure 5 and Figure S2). Since the reduction of N_2O to N_2 via the *nos*Z gene encoding the N_2O reductase is the only known microbial process that can consume N_2O,[53,54] the increased Chl-a concentration (i.e., algal biomass accumulation) likely inhibited both the denitrifying and N_2O-reducing bacteria. Gammaproteobacteria as the predominant representing denitrifiers harboring both *nir*S and *nos*Z genes were found to be the most abundant denitrifying population in lakes, mangroves, estuaries, and marine sediments.[55,56] Thus, the dominant presence of Gammaproteobacteria in Lake Taihu indicated that denitrifiers indeed played key roles during the N_2O production and consumption in the lake. A combination of isotopic and microbial analysis has been used to determine the denitrification and N_2O reduction activities in water and sediments.[57] However, no reasonable linear correlations were found between the $\delta^{15}N$ and $\delta^{18}O$ values of the NO_3−N and N_2O and their concentrations in spring, indicating restrained bacterial denitrification and N_2O consumption with increasing algal accumulation (Table 2 and Figure S3). As a result, the algal bloom inhibited the denitrification and N_2O reduction in the sediments, thus leading to low N_2O concentrations and N_2O fluxes. In contrast to the inhibitory effect of the algal bloom on the denitrifying communities, significant correlations were observed between the functional genes involved in the nitrification processes (*amo*ABC) and the N_2O concentration and $\delta^{15}N^{bulk}$ value (Figure 4), supporting the important role of nitrifying bacteria in N_2O production. This result is consistent with that of a recent study; that is, nitrifying microorganisms play a far more significant role in N_2O emissions in wetlands than was previously recognized.[58]

4.3. Quantitative Assessment of N_2O Production and Consumption. In this study, the most obvious spatiotemporal variations in the N_2O emissions occurred in summer and autumn, during which the lake shifted from a net N_2O sink to a net N_2O source and abnormally high N_2O concentrations occurred in the SV area. These two seasons were selected as representatives to quantitatively assess the relative contributions of nitrification and denitrification to the N_2O production, as well as the effect of N_2O consumption on the N_2O emissions. The isotopocule mapping results indicate that more than 50% of the lake N_2O was produced through microbial processes, among which approximately 90% was derived from denitrification (Table 3, Table S3, and Figure 5). However, a large amount of the N_2O produced was eliminated via N_2O reduction, and the higher degree of N_2O reduction led to lower N_2O concentrations and N_2O fluxes in the lake (Figure 5 and Figure S7a). The regulation of N_2O consumption on the lake's N_2O emissions is also supported by the calculated gross N_2O production and consumption rates, in which lower N_2O concentrations occurred with higher $N_2O_{consumption}$ values (Figure S7b). This observation can partially be explained by the fact that the measured N_2O concentrations are the net result of simultaneously occurring N_2O production and consumption processes; thus, intense N_2O consumption may respond to low N_2O concentrations.[19,38] In addition to the effect of N_2O consumption, the contributions of nitrification to the N_2O sources were observed to significantly increase with increasing N_2O concentration (Figure 5 and Table S3). These quantitative results are consistent with the qualitative evaluation based on the isotopic effects and the analysis of the key microbial functional genes (e.g., Table 2 and Figure 4),

https://doi.org/10.1021/acs.est.2c03992
Environ. Sci. Technol. XXXX, XXX, XXX−XXX

supporting the importance of nitrification to lake N_2O emissions. As a result, nitrification is suggested to be a key process that promotes N_2O production and regulates the temporal−spatial variations of N_2O emissions from Lake Taihu.

Denitrification has long been considered to be the dominant pathway of N_2O emissions in eutrophic Lake Taihu. Our comprehensive study supplements the current understanding of the N_2O dynamics and suggests that, although denitrification contributes most of the gross N_2O production in eutrophic shallow lakes, high N_2O consumption via microbial N_2O reduction would cause the lake to exhibit low N_2O levels. In contrast, nitrification seems to act as a key process promoting N_2O production and contributing to the lake as a source of N_2O emissions. The isotopocule mapping approach model yields the precise characteristics of the microbial N_2O production and consumption processes, which are easily ignored if the N_2O budget estimation is only based on *in situ* measurements of water N_2O concentrations and fluxes.

■ ASSOCIATED CONTENT

Supporting Information

The Supporting Information is available free of charge at https://pubs.acs.org/doi/10.1021/acs.est.2c03992.

Site description, N_2O concentration and flux, modified headspace-equilibrium method, IRMS calibration, and justification of isotopocule mapping approach, quantifying N_2O production and consumption, qualitative evaluation of N_2O production and consumption, structural equation models, microorganisms involved in N_2O production, and limitations and uncertainties (PDF)

■ AUTHOR INFORMATION

Corresponding Authors

Xia Liang − *State Key Laboratory of Estuarine and Coastal Research, East China Normal University, Shanghai 200241, People's Republic of China;* orcid.org/0000-0003-3882-5406; Email: xliang@sklec.ecnu.edu.cn

Lijun Hou − *State Key Laboratory of Estuarine and Coastal Research, East China Normal University, Shanghai 200241, People's Republic of China*; Email: ljhou@sklec.ecnu.edu.cn

Authors

Baoli Wang − *Institute of Surface-Earth System Science, Tianjin University, Tianjin 300072, People's Republic of China;* orcid.org/0000-0003-1437-6095

Dengzhou Gao − *State Key Laboratory of Estuarine and Coastal Research, East China Normal University, Shanghai 200241, People's Republic of China*

Ping Han − *State Key Laboratory of Estuarine and Coastal Research, East China Normal University, Shanghai 200241, People's Republic of China; School of Geographic Sciences, East China Normal University, Shanghai 200241, People's Republic of China;* orcid.org/0000-0001-6025-1651

Yanling Zheng − *State Key Laboratory of Estuarine and Coastal Research, East China Normal University, Shanghai 200241, People's Republic of China; School of Geographic Sciences, East China Normal University, Shanghai 200241, People's Republic of China;* orcid.org/0000-0002-8041-2843

Guoyu Yin − *State Key Laboratory of Estuarine and Coastal Research, East China Normal University, Shanghai 200241, People's Republic of China; School of Geographic Sciences, East China Normal University, Shanghai 200241, People's Republic of China;* orcid.org/0000-0002-8949-3731

Hongpo Dong − *State Key Laboratory of Estuarine and Coastal Research, East China Normal University, Shanghai 200241, People's Republic of China*

Yali Tang − *Engineering Research Center for Tropical and Subtropical Aquatic Ecological Engineering, Ministry of Education, Jinan University, Guangzhou 510632, People's Republic of China*

Complete contact information is available at: https://pubs.acs.org/10.1021/acs.est.2c03992

Author Contributions

#X.L. and B.W. contributed equally to the paper.

Notes

The authors declare no competing financial interest.

■ ACKNOWLEDGMENTS

This work was supported by the National Natural Science Foundation of China (41773076, 41725002, 42030411) and the Engineering Research Center for Tropical and Subtropical Aquatic Ecological Engineering, Ministry of Education, Jinan University, China (2021A0201). The authors acknowledge the kind help of our work team in field work and sample analysis. We also thank anonymous reviewers and the editors for their insightful comments.

■ REFERENCES

(1) Canadell, J. G.; Monteiro, P. M. S.; Costa, M. H.; Cotrim da Cunha, L.; Cox, P. M.; Eliseev, A. V.; Henson, S.; Ishii, M.; Jaccard, S.; Koven, C.; Lohila, A.; Patra, P. K.; Piao, S.; Rogelj, J.; Syampungani, S.; Zaehle, S.; Zickfeld, K.Global Carbon and other Biogeochemical Cycles and Feedbacks. In *Climate Change 2021: The Physical Science Basis. Contribution of Working Group I to the Sixth Assessment Report of the Intergovernmental Panel on Climate Change*; Masson-Delmotte, V., Zhai, P., Pirani, A., Connors, S. L., Péan, C., Berger, S., Caud, N., Chen, Y., Goldfarb, L., Gomis, M. I., Huang, M., Leitzell, K., Lonnoy, E., Matthews, J. B. R., Maycock, T. K., Waterfield, T.; Yelekçi, O., Yu, R., Zhou, B., Eds.; Cambridge University Press: 2021; pp 673−816.

(2) Soued, C.; Giorgio, P.; Maranger, R. Nitrous oxide sinks and emissions in boreal aquatic networks in Québec. *Nature Geosci.* **2016**, *9*, 116−120.

(3) Tian, H.; Xu, R.; Canadell, J. G.; Thompson, R. L.; Winiwarter, W.; Suntharalingam, P.; Davidson, E. A.; Ciais, P.; Jackson, R. B.; Janssens-Maenhout, G.; Prather, M. J.; Regnier, P.; Pan, N.; Pan, S.; Peters, G. P.; Shi, H.; Tubiello, F. N.; Zaehle, S.; Zhou, F.; Arneth, A.; Battaglia, G.; Berthet, S.; Bopp, L.; Bouwman, A. F.; Buitenhuis, E. T.; Chang, J.; Chipperfield, M. P.; Dangal, S. R. S.; Dlugokencky, E.; Elkins, J. W.; Eyre, B. D.; Fu, B.; Hall, B.; Ito, A.; Joos, F.; Krummel, P. B.; Landolfi, A.; Laruelle, G. G.; Lauerwald, R.; Li, W.; Lienert, S.; Maavara, T.; MacLeod, M.; Millet, D. B.; Olin, S.; Patra, P. K.; Prinn, R. G.; Raymond, P. A.; Ruiz, D. J.; Werf, G. R.; Vuichard, N.; Wang, J.; Weiss, R. F.; Wells, K. C.; Wilson, C.; Yang, J.; Yao, Y. A comprehensive quantification of global nitrous oxide sources and sinks. *Nature* **2020**, *586*, 248−256.

(4) Kato, T.; Toyoda, S.; Yoshida, N.; Tang, Y. H.; Wada, E. Isotopomer and isotopologue signatures of N_2O produced in alpine ecosystems on the Qinghai-Tibetan Plateau. *Rapid Commun. Mass Spectrom.* **2013**, *27*, 1517−1526.

(5) Li, Q.; Wang, F.; Yu, Q.; Yan, W.; Li, X.; Lv, S. xsDominance of nitrous oxide production by nitrification and denitrification in the

shallow Chaohu Lake, Eastern China: insight from isotopic characteristics of dissolved nitrous oxide. *Environ. Pollut.* **2019**, *255*, 113212.
(6) Beaulieu, J. J.; Tank, J. L.; Hamilton, S. K.; Wollheim, W. M.; Hall, R. O.; Mulholland, P. J.; Peterson, B. J.; Ashkenas, L. R.; Cooper, L. W.; Dahm, C. N.; Dodds, W. K.; Grimm, N. B.; Johnson, S. L.; McDowell, W. H.; Poole, G. C.; Valett, H. M.; Arango, C. P.; Bernot, M. J.; Burgin, A. J.; Crenshaw, C. L.; Helton, A. M.; Johnson, L. T.; O'Brien, J. M.; Potter, J. D.; Sheibley, R. W.; Sobota, D. J.; Thomas, S. M. Nitrous oxide emission from denitrification in stream and river networks. Proc. *Natl. Acad. Sci. U.S.A.* **2011**, *108*, 214−219.
(7) Rissanen, A. J.; Tiirola, M.; Hietanen, S.; Ojala, A. Interlake variation and environmental controls of denitrification across different geographical scales. *Aquat. Microb. Ecol.* **2013**, *69*, 1−16.
(8) Nelson, W. C.; Graham, E. B.; Crump, A. R.; Fansler, S. J.; Arntzen, E. V.; Kennedy, D. W.; Stegen, J. C.Temporal dynamics of nitrogen cycle gene diversity in a hyporheic microbiome.*bioRxiv*, 2019; 722785
(9) Lauerwald, R.; Regnier, P.; Figueiredo, V.; Enrich-Prast, A.; Bastviken, D.; Lehner, B.; Maavara, T.; Raymond, P. Natural lakes are a minor global source of N_2O to the atmosphere. *Global Biogeochem. Cycles* **2019**, *33*, 1564−1581.
(10) Yao, Y.; Tian, H.; Shi, H.; Pan, S.; Xu, R.; Pan, N.; Canadell, J. Increased global nitrous oxide emissions from streams and rivers in the Anthropocene. *Nat. Clim. Chang.* **2020**, *10*, 138−142.
(11) Toyoda, S.; Yano, M.; Nishimura, S.; Akiyama, H.; Hayakawa, A.; Koba, K.; Sudo, S.; Yagi, K.; Makabe, A.; Tobari, Y.; Ogawa, N. O.; Ohkouchi, N.; Yamada, K.; Yoshida, N. Characterization and production and consumption processes of N_2O emitted from temperate agricultural soils determined via isotopomer ratio analysis. *Global Biogeochem. Cycles* **2011**, *25*, GB2008.
(12) Hu, H.; Chen, D.; He, J. Microbial regulation of terrestrial nitrous oxide formation: understanding the biological pathways for prediction of emission rates. *FEMS Microbiol. Rev.* **2015**, *39*, 729−749.
(13) Lewicka-Szczebak, D.; Augustin, J.; Giesemann, A.; Well, R. Quantifying N_2O reduction to N_2 based on N_2O isotopocules-validation with independent methods (helium incubation and ^{15}N gas flux method). *Biogeosciences* **2017**, *14*, 711−732.
(14) Toyoda, S.; Yoshda, N.; Koba, K. Isotopocule analysis of biologically produced nitrous oxide in various environments. *Mass Spectrom. Rev.* **2017**, *36*, 135−160.
(15) Lewicka-Szczebak, D.; Lewicki, M. P.; Well, R. N_2O isotope approaches for source partitioning of N_2O production and estimation of N_2O reduction-validation with the ^{15}N gas-flux method in laboratory and field studies. *Biogeosciences* **2020**, *17*, 5513−5537.
(16) Koba, K.; Osaka, K.; Tobari, Y.; Toyoda, S.; Ohte, N.; Katsuyama, M.; Suzuki, N.; Itoh, M.; Yamagishi, H.; Kawasaki, M.; Kim, S. J.; Yoshida, N.; Nakajima, T. Biogeochemistry of nitrous oxide in groundwater in a forested ecosystem elucidated by nitrous oxide isotopomer measurements. *Geochim. Cosmochim. Acta* **2009**, *73*, 3115.
(17) Gao, D.; Hou, L.; Liu, M.; Li, X.; Zheng, Y.; Yin, G.; Wu, D.; Yang, Y.; Han, P.; Liang, X.; Dong, H. Mechanisms responsible for N_2O emissions from intertidal soils of the Yangtze Estuary. *Sci. Total Environ.* **2020**, *716*, 137073.
(18) Gao, D.; Hou, L.; Liu, M.; Zheng, Y.; Yin, G.; Niu, Y. N_2O emission dynamics along an intertidal elevation gradient in a subtropical estuary: Importance of N_2O consumption. *Environ. Res.* **2022**, *205*, 112432.
(19) Quick, A. M.; Reeder, W. J.; Farrell, T. B.; Tonina, D.; Feris, K. P.; Benner, S. G. Nitrous oxide from streams and rivers: a review of primary biogeochemical pathways and environmental variables. *Earth Sci. Rev.* **2019**, *191*, 224−262.
(20) Bourbonnais, A.; Letscher, R. T.; Bange, H. W.; Échevin, V.; Larkum, J.; Mohn, J.; Yoshida, N.; Altabet, M. A. N_2O production and consumption from stable isotopic and concentration data in the Peruvian coastal upwelling system. *Global Biogeochem. Cycles* **2017**, *31*, 678−698.
(21) Zhao, S.; Wang, X.; Pan, H.; Wang, Y.; Zhu, G. High N_2O reduction potential by denitrification in the nearshore site of a riparian zone. *Sci. Total Environ.* **2022**, *813*, 152458.
(22) Salk, K. R.; Ostrom, P. H.; Biddanda, B. A.; Weinke, A. D.; Kendall, S. T.; Ostrom, N. E. Ecosystem metabolism and greenhouse gas production in a mesotrophic northern temperate lake experiencing seasonal hypoxia. *Biogeochemistry* **2016**, *131*, 303−319.
(23) Salk, K. R.; Ostrom, N. E. Nitrous oxide in the Great Lakes: insights from two trophic extremes. *Biogeochemistry* **2019**, *144*, 233−243.
(24) Qin, B.; Xu, P.; Wu, Q.; Luo, L.; Zhang, Y. Environmental issues of Lake Taihu, China. *Hydrobiologia* **2007**, *581*, 3−14.
(25) Xiao, Q.; Xu, X.; Zhang, M.; Duan, H.; Hu, Z.; Wang, W.; Xiao, W.; Lee, X. Coregulation of nitrous oxide emissions by nitrogen and temperature in China's third largest freshwater lake (Lake Taihu). *Limnol Oceanogr.* **2019**, *64*, 1070−1086.
(26) Wang, S.; Liu, C.; Yeager, K. M.; Wan, G.; Li, J.; Tao, F.; Lu, Y.; Liu, F.; Fan, C. The spatial distribution and emission of nitrous oxide (N_2O) in a large eutrophic lake in eastern China: Anthropogenic effects. *Sci. Total Environ.* **2009**, *407*, 3330−3337.
(27) Song, K.; Senbati, Y.; Li, L.; Zhao, X.; Xue, Y.; Deng, M. Distinctive microbial processes and controlling factors related to indirect N_2O emission from agricultural and urban rivers in Taihu watershed. *Environ. Sci. Technol.* **2022**, *56*, 4642.
(28) Zhu, L.; Shi, W.; Dam, B. V.; Kong, L.; Yu, J.; Qin, B. Algal accumulation decreases sediment nitrogen removal by uncoupling nitrification-denitrification in shallow eutrophic lakes. *Environ. Sci. Technol.* **2020**, *54*, 6194−6201.
(29) China, E. P. A.*Environmental Quality Standards for Surface Water of the People's Republic of China.*; Ministry of Environmental Protection of the People's Republic of China: 2002.
(30) Liang, X.; Xing, T.; Li, J.; Wang, B.; Wang, F.; He, C.; Hou, L.; Li, S. Control of the hydraulic load on nitrous oxide emissions from cascade reservoirs. *Environ. Sci. Technol.* **2019**, *53*, 11745−11754.
(31) Goldenfum, J. A.*GHG Measurement Guidelines for Freshwater Reservoirs Derived from The UNESCO/IHA Greenhouse Gas Emissions from Freshwater Reservoirs Research Project*; International Hydropower Association: 2018.
(32) Mengis, M.; Gachter, R.; Wehrli, B. Sources and sinks of nitrous oxide (N_2O) in deep lakes. *Biogeochemistry* **1997**, *38*, 281−301.
(33) Macintyre, S.; Wanninkhof, R.; Chanton, J. P.Trace gas exchange across the air-water interface in freshwater and coastal marine environments. In: *Biogenic Trace Gases: Measuring Emissions from Soil and Water*; Matson, P. A., Harriss, R. C., Eds.; Blackwell: 1995; pp 52−97.
(34) Yuan, J.; Xiang, J.; Liu, D.; Kang, H.; He, T.; Kim, S.; Lin, Y.; Freeman, C.; Ding, W. Rapid growth in greenhouse gas emissions from the adoption of industrial-scale aquaculture. *Nat. Clim. Chang.* **2019**, *9*, 318−322.
(35) Liu, D.; Fang, Y.; Tu, Y.; Pan, Y. Chemical Method for Nitrogen Isotopic Analysis of Ammonium at Natural Abundance. *Anal. Chem.* **2014**, *86*, 3787−3792.
(36) Zhu, J.; Yu, L.; Bakken, L. R.; Mørkved, P. T.; Mulder, J.; Dörsch, P. Controlled induction of denitrification in *Pseudomonas aureofaciens*: A simplified denitrifier method for dual isotope analysis in NO_3^-. *Sci. Total Environ.* **2018**, *633*, 1370−1378.
(37) Toyoda, S.; Yoshida, N. Determination of nitrogen isotopomers of nitrous oxide on a modified isotope ratio mass spectrometer-analytical chemistry. *Anal. Chem.* **1999**, *71*, 4711−4718.
(38) Wenk, C. B.; Frame, C. H.; Koba, K.; Casciotti, K. L.; Veronesi, M.; Niemann, H.; Schubert, C. J.; Yoshida, N.; Toyoda, S.; Makabe, A.; Zopfi, J.; Lehmann, M. F. Differential N_2O dynamics in two oxygen-deficient lake basins revealed by stable isotope and isotopomer distributions. *Limnol. Oceanogr.* **2016**, *61*, 1735−1749.
(39) Lewicka-Szczebak, D.; Dyckmanns, J.; Kaiser, J.; Marca, A.; Augustin, J.; Well, R. Oxygen isotope fractionation during N_2O production by soil denitrification. *Biogeosciences* **2016**, *13*, 1129−1144.

https://doi.org/10.1021/acs.est.2c03992
Environ. Sci. Technol. XXXX, XXX, XXX−XXX

(40) Wu, D.; Well, R.; Cárdenas, L. M.; Fuß, R.; Lewicka-Szczebak, D.; Köster, J. R.; Brüggemann, N.; Bol, R. Quantifying N_2O reduction to N_2 during denitrification in soils via isotopic mapping approach: model evaluation and uncertainty analysis. *Environ. Res.* **2019**, *179*, 108806.
(41) Verhoeven, E.; Barthel, M.; Yu, L.; Celi, L.; Said-Pullicino, D.; Sleutel, S.; Lewicka-Szczebak, D.; Six, J.; Decock, C. Early season N_2O emissions under variable water management in rice systems: source-partitioning emissions using isotope ratios along a depth profile. *Biogeosciences* **2019**, *16*, 383−408.
(42) *Measuring Emission of Agricultural Greenhouse Gases and Developing Mitigation Options Using Nuclear and Related Techniques*; Zaman, M., Heng, L., Müller, C., Eds.; Springer Nature: 2021.
(43) Chen, S.; Zhou, Y.; Chen, Y.; Gu, J. fastp: an ultra-fast all-in-one FASTQ preprocessor. *Bioinformatics* **2018**, *34*, i884−i890.
(44) Fu, L.; Niu, B.; Zhu, Z.; Wu, S.; Li, W. CD-HIT: accelerated for clustering the next-generation sequencing data. *Bioinformatics* **2012**, *28*, 3150−3152.
(45) Buchfink, B.; Xie, C.; Huson, D. H. Fast and sensitive protein alignment using DIAMOND. *Nat. Methods* **2015**, *12*, 59−60.
(46) Müller, B.; Thoma, R.; Baumann, K. B. L.; Callbeck, C. M.; Schubert, C. J. Nitrogen removal processes in lakes of different trophic states from on-site measurements and historic data. *Aquat. Sci.* **2021**, *83*, 37.
(47) Webb, J. R.; Hayes, N. M.; Simpson, G. L.; Leavitt, P. R.; Baulch, H. M.; Finlay, K. Wide spread nitrous oxide undersaturation in farm waterbodies creates an unexpected green house gas sink. *Proc. Natl. Acad. Sci. U.S.A.* **2019**, *116*, 9814−9819.
(48) Xing, P.; Tao, Y.; Luo, J.; Wang, L.; Li, B.; Li, H.; Wu, Q. Stratification of microbiomes during the holomictic period of Lake Fuxian, an alpine monomictic lake. *Limnol Oceanogr.* **2020**, *65*, S134−S148.
(49) Mathieu, O.; Lévêque, J.; Hénault, C.; Ambus, P.; Milloux, M. J.; Andreux, F. Influence of ^{15}N enrichement on the net isotopic fractionation factor during the reduction of nitrate to nitrous oxide in soil. *Rapid Commun. Mass Sp.* **2007**, *21*, 1447−1451.
(50) Botrel, M.; Bristow, L. A.; Altabet, M. A.; Gregory-Eaves, I.; Maranger, R. Assimilation and nitrification in pelagic waters: insights using dual nitrate stable isotopes ($\delta^{15}N$, $\delta^{18}O$) in a shallow lake. *Biogeochemistry* **2017**, *135*, 221−237.
(51) Yamagishi, H.; Westley, M. B.; Popp, B. N.; Toyoda, S.; Yoshida, N.; Watanabe, S.; Koba, K.; Yamanaka, Y. Role of nitrification and denitrification on the nitrous oxide cycle in the eastern tropical North Pacific and Gulf of California. *J. Geophys. Res.* **2007**, *112*, G02015.
(52) Wang, F.; Chen, N.; Yan, J.; Lin, J.; Guo, W.; Cheng, P.; Liu, Q.; Huang, B.; Tian, Y. Major processes shaping mangroves as inorganic nitrogen sources or sinks: Insights from a multidisciplinary study. *J. Geophys. Res. Biogeosci.* **2019**, *124*, 1194−1208.
(53) Jones, C. M.; Graf, D. R.; Bru, D.; et al. The unaccounted yet abundant nitrous oxide-reducing microbial community: a potential nitrous oxide sink. *ISME J.* **2013**, *7*, 417−426.
(54) Suenaga, T.; Riya, S.; Hosomi, M.; Terada, A. Biokinetic characterization and activities of N_2O-reducing bacteria in response to various oxygen levels. *Front. Microbiol.* **2018**, *9*, 697.
(55) Baskaran, V.; Prabavathy, V. R. Diverse key nitrogen cycling genes *nifH*, *nirS* and *nosZ* associated with Pichavaram mangrove rhizospheres as revealed by culture-dependent and culture-independent analyses. *Arch. Microbiol.* **2022**, *204*, 109.
(56) Percent, S. F.; Frischer, M. E.; Vescio, P. A.; Duffy, E. B.; Milano, V.; McLellan, M.; Stevens, B. M.; Boylen, C. W.; Nierzwicki-Bauer, S. A. Bacterial community structure of acid-impacted lakes: what controls diversity? *Appl. Environ. Microbiol.* **2008**, *74*, 1856−68.
(57) Masta, M.; Espenberg, M.; Gadegaonkar, S. S.; Pärn, J.; Sepp, H.; Kirsimäe, K.; Sgouridis, F.; Müller, C.; Mander, Ü. Integrated isotope and microbiome analysis indicates dominance of denitrification in N2O production after rewetting of drained fen peat. *Biogeochemistry* **2022**.
(58) Bahram, M.; Espenberg, M.; Pärn, J.; Lehtovirta-Morley, L.; Anslan, S.; Kasak, K.; Kõljalg, U.; Liira, J.; Maddison, M.; Moora, M.; Niinemets, Ü.; Öpik, M.; Pärtel, M.; Soosaar, K.; Zobel, M.; Hildebrand, F.; Tedersoo, L.; Mander, Ü. Structure and function of the soil microbiome underlying N_2O emissions from global wetlands. *Nat. Commun.* **2022**, *13*, 1430.

https://doi.org/10.1021/acs.est.2c03992
Environ. Sci. Technol. XXXX, XXX, XXX−XXX